PERGAMON

International Journal of Heat and Mass Transfer 44 (2001) 1527–1541

International Journal of HEAT and MASS TRANSFER

www.elsevier.com/locate/ijhmt

Dynamics of evaporating drops. Part II: free oscillations

Farzad Mashayek *

Department of Mechanical Engineering, University of Illinois at Chicago, 842 West Taylor Street, Chicago, IL 60607, USA

Received 24 August 1999; received in revised form 6 June 2000

Abstract

Free oscillations of evaporating drops are investigated using a combination of numerical and theoretical analyses. The investigation is based on an evaporation model that expresses the mass flux as a function of the surface curvature and is valid for surface amplitudes up to 10% of the drop radius. The results show that, the period of oscillation is decreased by evaporation, however, the dominant mode of oscillation remains the same as that for a non-evaporating drop. For low evaporation rates, it is shown that the recoil force is responsible for modifications in the period. At high evaporation rates, the period of oscillation also varies significantly in time, due to the decrease of the drop size. The theoretical analysis is mainly concerned with infinitesimal-amplitude oscillations via invoking simplifying assumptions which are supported by numerical results. Closed-form expressions are derived for the period and the kinetic energy of the drop. The predictions of the theory are compared with the results of the numerical simulations and excellent agreements are observed. The effect of oscillations on the rate of evaporation is also investigated, and it is shown that the rate of evaporation decreases for an oscillating drop as compared to a deformed but non-oscillating drop.

1. Introduction

The overall objective of this work is to investigate the oscillations of evaporating drops and its impact on the rate of evaporation. In Part I [1] of this study, we showed that for a drop at its boiling temperature, and with a large density ratio, the liquid and the gas phases may be studied separately. The results of the gas phase are presented in Part I, where a model is introduced to describe the rate of evaporation of a deformed drop as a function of its surface curvature. Here, we implement this model to investigate free oscillations of an evaporating drop at small amplitudes.

Oscillations of a drop constitute one of the classical problems in fluid mechanics. One of the early studies is due to Rayleigh [2] who presents an analytical solution for the infinitesimal-amplitude oscillations of inviscid drops in vacuum. The normal-mode technique is used to find the frequency of oscillation of various spherical harmonics which are also referred to as ''oscillation modes''. The viscous effects and forces due to self-gravitation are introduced into this problem by Lamb [3] and Chandrasekhar [4]. Later, Reid [5] shows that for arbitrary values of viscosity the results are the same for self-gravitation and surface tension. Prosperetti [6] considers the initial value problem of infinitesimal-amplitude oscillations of viscous drops and shows that the frequency of oscillations decreases with the decrease of the Reynolds number. A nonlinear analytical solution for moderate-amplitude oscillations of inviscid drops is provided by Tsamopolous and Brown [7] who find that the frequency of oscillation decreases with the square of the initial amplitude.

Early numerical simulations of drop oscillations have been carried out by Foote [8] and Alonso [9] using marker-and-cell method for a limited number of oscillations. Boundary integral technique is implemented by Lundgren and Mansour [10] to study the large-amplitude oscillations of inviscid drops as well as drops with weak viscous effects. Recently, Mashayek and Ashgriz [11] have implemented the finite element method to study oscillations of a drop with and without internal circulation. The experimental studies in this field can be exemplified by the work of Trinh and Wang [12] who

* Tel.: (312) 996-5317; fax: (312) 413-0447.
E-mail address: mashaye@uic.edu (F. Mashayek).

0017-9310/01/$ - see front matter
PII: S0017-9310(00)00200-3

Nomenclature

a	mean drop radius
B	$C_{pg}(T_\infty - T_b)/L_v$ transfer number
C_p	specific heat
E_k	kinetic energy
F_n	$(3n+2)/2[n(n+1)+2]$
h	spine function
$\mathbf{I}$	identity tensor
k	thermal conductivity coefficient
$\mathscr{K}$	drop surface curvature
L_v	latent heat of evaporation
$\dot{m}$	mass flux
$\dot{M}$	rate of change of drop mass
n	mode of oscillation
$\mathbf{n}$	outward unit normal vector
p	pressure
P_n	Legendre polynomial of degree n
r	radial (cylindrical) coordinate
r_0	initial radius of the non-perturbed drop
R_n	volume correction factor
Re_l	$(1/\nu_l)(\sigma r_0/\rho_l)^{1/2}$ liquid Reynolds number
t	time
T	temperature
$\mathbf{T}$	stress tensor
$\mathbf{u}$	(u,v) velocity vector
V	drop volume
z	axial coordinate

Greek symbols

α	β^2/λ
β	non-dimensional rate of evaporation
Γ	decay factor
ϵ_n	surface disturbance amplitude for mode n
ζ	phase shift
λ	ρ_g/ρ_l density ratio
ν	kinematic viscosity
ρ	density
σ	surface tension coefficient
τ	oscillation period
ϕ	inclination angle from drop axis
Φ	velocity potential
χ	non-dimensional mass flux
ω	non-dimensional oscillation frequency

Subscripts

0	initial value
b	boiling condition
eq	equilibrium
g	gas
l	liquid
ne	non-evaporating
∞	gas condition far from drop surface

Symbol

ϱ	non-dimensional radius of the spherical drop

show an amplitude dependency of the frequency at large amplitudes. Becker et al. [13] study oscillations of drops generated from the breakup of a liquid jet. Wang et al. [14] report the results from experiments on oscillations of low-viscosity drops performed on board of Space shuttle and verify the inviscid frequency shift, due to nonlinearity, as predicted in [7]. Recently, Trinh et al. [15] have studied large-amplitude oscillations of drops and bubbles surrounded by another immiscible liquid.

Although the literature review above is brief, it does indicate that free oscillations of evaporating drops has not been the subject of a detailed investigation. These oscillations can become important in atomization systems where the liquid is first disintegrated into small ligaments which then oscillate towards the attainment of an equilibrium spherical shape. If these ligaments/drops are exposed to a hot gas then the heat and mass transfer could be affected by oscillations. Another possible implication of the results of this study could be found in the measurement of the surface tension coefficient using the drop oscillation period. In this situation, modifications in the period of oscillation due to evaporation can influence the accurate measurement of the surface tension coefficient. These modifications can be predicted by the present study. In this paper, we first implement the evaporation model developed in Part I to study the oscillations of evaporating drops via both numerical and theoretical analysis in Section 2. A discussion of the effects of oscillations on the rate of evaporation is then presented in Section 3. A summary and some concluding remarks are provided in Section 4.

2. Oscillations of evaporating drops

The governing equations are the continuity and momentum equations for the liquid phase which are described from Part I as:

$$\nabla \cdot \mathbf{u}_l = 0, \tag{2.1}$$

$$\frac{\partial \mathbf{u}_l}{\partial t} + \mathbf{u}_l \cdot \nabla \mathbf{u}_l = \frac{1}{Re_l} \nabla \cdot \mathbf{T}_l, \tag{2.2}$$

where $\mathbf{T}_l = -p_l \mathbf{I} + [\nabla \mathbf{u}_l + (\nabla \mathbf{u}_l)^T]$ for Newtonian fluid. All the variables are non-dimensionalized using the initial radius of the spherical drop, r_0, and a characteristic time, $(\rho_l r_0^3/\sigma)^{1/2}$. Note that no energy equation is considered for the liquid phase as the drop is assumed to be at its boiling temperature. This also eliminates the possibility of thermocapillary flows within the drop.

The non-dimensional stress balance on the interface is expressed as:

$$\mathbf{T}_1 \cdot \mathbf{n} = Re_1 \left(\mathscr{K} + \alpha \left[F_n \mathscr{K} + \frac{2}{\varrho}(1 - F_n) \right]^2 \right) \mathbf{n}, \tag{2.3}$$

where the surface curvature, $\mathscr{K}$, is calculated from the spine function, $h(\phi)$, which describes the surface of the drop (Fig. 1(a)):

$$\mathscr{K} = -\frac{h^2 + 2h_\phi^2 - hh_{\phi\phi}}{(h_\phi^2 + h^2)^{1.5}} - \frac{h - \cot\phi h_\phi}{h(h_\phi^2 + h^2)^{0.5}}, \tag{2.4}$$

and

$$\alpha = \frac{\beta^2}{\lambda}, \quad \lambda = \frac{\rho_g}{\rho_1}, \quad \beta = \frac{1}{2}(\rho_1 r_0 \sigma)^{-(1/2)} \left(\frac{k_g}{C_{pg}} \right) \ln(1 + B). \tag{2.5}$$

In writing (2.3), we have implemented the evaporation model from Part I:

$$\chi = \left[F_n \left(\mathscr{K} - \frac{2}{\varrho} \right) + \frac{2}{\varrho} \right] \beta, \quad F_n = \frac{3n + 2}{2[n(n + 1) + 2]}. \tag{2.6}$$

As a result of non-dimensionalization, the parameters affecting oscillations of an evaporating drop reduce to Re_1, β, and λ. In this section, we investigate the effects of these parameters and the mode of oscillations via numerical simulation and normal-mode analysis. It must be emphasized that, due to the limitation imposed by the evaporation model, only small-amplitude oscillations are considered.

2.1. Simulation

The non-dimensional continuity and momentum equations (2.1) and (2.2) are solved to investigate the oscillations of an axisymmetric evaporating drop subjected to boundary conditions

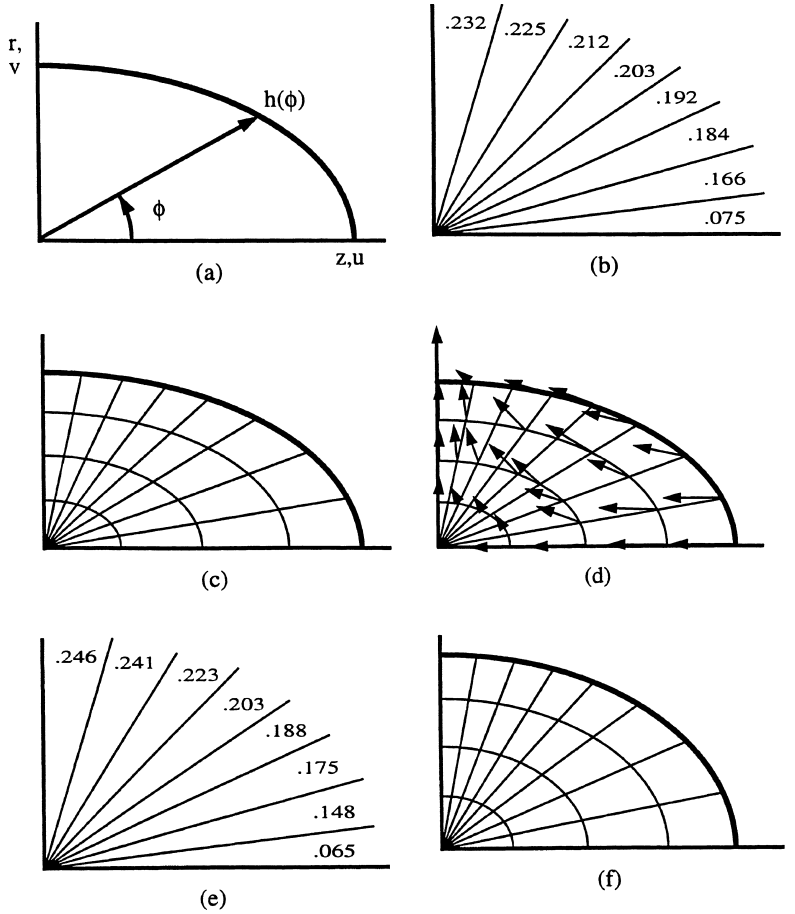

Fig. 1. Illustration of various steps involved in SFM: (a) definition of the initial interface by spine function $h(\phi)$; (b) subdivision of the domain into subvolumes and description of the subvolume quantity; (c) mesh generation; (d) calculation of the velocity field; (e) advection of the liquid and calculation of the new subvolume quantities; (f) reconstruction of the new interface and generation of finite element mesh.

$$\frac{\partial u_l}{\partial r} = 0, \quad v_l = 0 \quad \text{at } r = 0. \tag{2.7}$$

For even-mode oscillations symmetry boundary conditions are also implemented on the plane of symmetry

$$u_l = 0, \quad \frac{\partial v_l}{\partial z} = 0 \quad \text{at } z = 0. \tag{2.8}$$

The surface of the drop is initially perturbed from its spherical shape using spherical harmonics

$$h(\phi) = R_n[1 + \epsilon_n P_n(\cos\phi)], \tag{2.9}$$

where $P_n(\cos\phi)$ is the Legendre polynomial of degree n, ϵ_n the amplitude of the disturbance, and R_n is used to maintain the volume of the drop constant when ϵ_n is varied. The relations for R_n are given in Part I.

The governing equations are solved using a Galerkin finite element method with penalty function formulation as described in Part I. The interface is tracked using the spine-flux method (SFM) [16]. SFM implicitly accounts for the kinematic boundary condition on the interface, and its basic constituents are illustrated in Fig. 1. To follow the motion of the interface (Fig. 1(a)), the fluid domain is divided into small subvolumes which are separated by spines (Fig. 1(b)). The location of the interface is given by its distance from the origin of the coordinate system along these spines. At the end of each time step fluxes of the fluid from each subvolume to its neighboring subvolumes are calculated using the velocity field (Fig. 1(d)) determined by the finite element solution of the governing equations. After the new volume in each subvolume is calculated (Fig. 1(e)), a linear approximation is used to describe the part of the interface confined within every pair of neighboring subvolumes. With the knowledge of the volumes of fluid inside these subvolumes, the constants of the line are determined and intersection of the interface with the common spine between the neighboring subvolumes is obtained. Repeating this procedure for all the spines yields the location of the interface which is then used to generate a new finite element mesh (Fig. 1(f)) for the next time step.

Due to the nature of SFM, its application for the simulation of evaporating drops is straightforward. With the knowledge of evaporation rate, the volume change

$$\delta V_e = \pi(h_i + h_{i+1})\beta\left[F_n\mathscr{K} + \frac{2}{\varrho}(1 - F_n)\right]\delta l\ \delta t, \tag{2.10}$$

for each subvolume is calculated for the time increment δt, and is accounted for when updating the volume of the fluid inside the subvolume during the step shown in Fig. 1(e). In (2.10), δl denotes the length of the interface confined within the subvolume.

Preliminary simulations have been performed with different mesh sizes and time increments in order to establish the accuracy of the results for various cases. Table 1 shows the variation of the first period of oscillation with mesh size for a typical drop released from a fourth spherical harmonic initial (indicated by subscript '0') surface disturbance. For this case, $\epsilon_{40} = 0.05$, $Re_l = 100$, $\beta = 2 \times 10^{-4}$, and $\lambda = 10^{-7}$. The table shows that a reasonable accuracy in calculating the period may be achieved using 34 elements in the peripheral and seven elements in the radial directions. In general, the results are more sensitive to the number of elements in the peripheral direction than to that in the radial direction. This is expected as the increase of the number of elements in the peripheral direction also improves the accuracy in the representation of the interface. Mashayek and Ashgriz [16] show that SFM is second-order accurate, i.e., the error in interface reconstruction decreases quadratically with the decrease of the node spacing in the peripheral direction.

In analyzing the results of the simulations, it is instructive to consider the temporal variations of the amplitudes (A_m) of the primary input and its harmonics. This is accomplished by decomposing the surface of the drop, $h(\phi, t)$, into its linear modes:

$$h(\phi, t) = \varrho(t)\left[1 + \sum A_m(t)P_m(\cos\phi)\right], \quad m = 0, 1, 2, \ldots, \tag{2.11}$$

where $\varrho(t)$ is the radius of the equivalent spherical drop at time t. The coefficients $A_m(t)$ are determined from (2.11) using the orthogonality of the Legendre polynomials and numerical integration.

2.1.1. Low evaporation rate

In order to relate the magnitude of non-dimensional evaporation rates to values of the physical variables, here we consider a heptane drop in air as an example. We assume that properties of heptane are fixed at $\rho_l = 649.4$ kg/m^3, $\sigma = 0.0148$ N/m, and $L_v = 361.8$ kJ/kg, as typical values. Properties of air vary with temperature, therefore, to provide a better estimate we use $C_{pg} = 1.006$–1.099 kJ/kg°C and $k_g = 0.03$–0.057 W/m°C for air at various temperatures and atmospheric pressure. We also choose $r_0 = 60$ μm for the initial radius of the spherical drop. Substituting these values in (2.5), we can estimate the non-dimensional

Table 1
Variation of the first period of oscillation with mesh size from a typical convergence study. $\epsilon_{40} = 0.05$, $Re_l = 100$, $\beta = 2 \times 10^{-4}$, and $\lambda = 10^{-7}$

Mesh size	22×7	26×7	30×7	34×7	38×7	30×9
First period	0.615	0.613	0.612	0.611	0.611	0.612

evaporation rate β for various values of the temperature difference $\Delta T = T_\infty - T_b$ as shown in Table 2. It must be emphasized that the values given in the table are only representative and may vary in a real case. Also shown in the table is the parameter $\%\Delta V/V_0 = 100 \times (V_0 - V)/V_0$, which indicates the percent relative change in the volume (V) of a spherical drop with respect to its value before evaporation (V_0). The instantaneous volume $V = 4\pi\varrho^3/3$ has been calculated using $\varrho(t) = (1 - 4\beta t)^{1/2}$ which describes the temporal variation of the radius of a spherical drop. To calculate the values shown in Table 2, $t = 2.221$ has been used as a typical value which is the prediction of the inviscid theory for the period of oscillations of a non-evaporating drop released from a second spherical harmonic surface perturbation. It is observed that evaporation rates $O(10^{-4})$ are easily feasible with temperature differences around 60°C. However, the change in the volume of the drop for this rate of evaporation is too small to be considered significant for most laboratory experiments. It is also noted that the values of B in Table 2 are within the range used in simulations in Part I. In this section, we consider evaporation rates listed in Table 2. Higher evaporation rates, resulting in large changes in the volume of the drop, are discussed in Section 2.1.2.

Fig. 2 shows the temporal variations of the amplitude of the primary mode P_2 for a drop released with $\epsilon_{20} = 0.05$ and $Re_l = 100$. Both non-evaporating ($\beta = 0$) and evaporating ($\beta = 2 \times 10^{-4}$, $\lambda = 10^{-7}$) cases are considered. The figure clearly shows that, while oscillations remain periodic, the frequency is increased by evaporation. Similar observations were made for all of the harmonics and all of the cases considered in this study. This suggests that the behavior of evaporating drops (similar to non-evaporating drops) oscillating at small amplitudes may be characterized by the primary input only. Therefore, in analyzing the results we will only consider the primary input.

A review of formulation in Part I reveals that evaporation can affect oscillations: (i) by decreasing the size of the drop; and/or (ii) through the recoil force appearing in the normal stress boundary condition. Table 2 indicates that changes in the drop size are not very significant for cases considered in this subsection.

Table 2
Typical values for B, β, and $\%\Delta V/V_0$ ($\Delta V = V_0 - V$) as a function of $\Delta T = T_\infty - T_b$ for heptane drops in air using the property values listed in the text

ΔT (°C)	B	β	$\%\Delta V/V_0$
30	0.084	5×10^{-5}	0.067
60	0.167	1×10^{-4}	0.133
110	0.310	2×10^{-4}	0.27
250	0.735	5×10^{-4}	0.67
500	1.519	1×10^{-3}	1.33

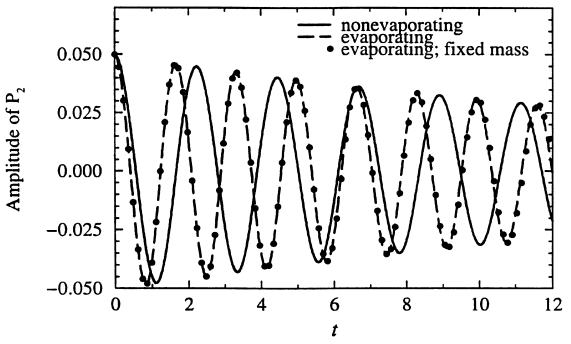

Fig. 2. Temporal variations of the amplitude of the primary input P_2 for a drop released with $\epsilon_{20} = 0.05$ and $Re_l = 100$. For evaporating cases $\beta = 2 \times 10^{-4}$ and $\lambda = 10^{-7}$.

This suggests that the recoil force should be responsible for modifications observed in the period of oscillations. This may be examined by keeping the size of the drop unchanged in the numerical simulation while imposing the recoil force. The temporal evolution of the primary input for this case, labeled with "fixed mass", is also shown in Fig. 2. It is clearly observed in the figure that the result for the evaporating case without size change is virtually identical to the result from the evaporating case. This verifies that, for low evaporation rates, the recoil force is the cause of the changes in the period of oscillation. A theoretical description will be given in Section 2.2.

Fig. 3 shows the variation of the period of oscillation with the density ratio for a drop with $\epsilon_2 = 0.05$ and $Re_l = 100$. The values of the period shown in the figure are the average of the first three periods to reduce the effects of the initial conditions. The first case is for $\beta = 2 \times 10^{-4}$ which, according to Table 2, corresponds to $\Delta T \simeq 110$°C. It is observed that as the gas density is decreased the period of oscillations also decreases. For $\lambda = 3 \times 10^{-6}$, the change in the period of oscillation is

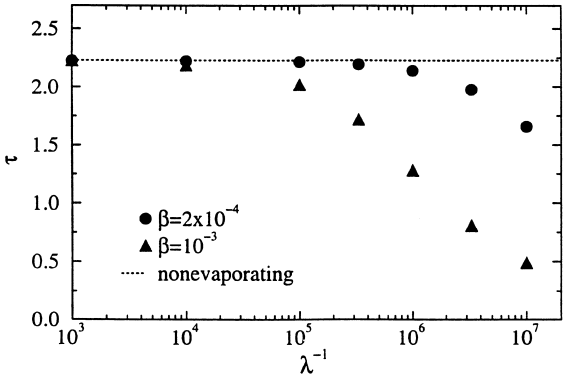

Fig. 3. Variations of the period of oscillation with density ratio for an evaporating drop with $\epsilon_{20} = 0.05$ and $Re_l = 100$.

about 1.5% which could be detectable via laboratory experiments. Further decrease in the gas density results in more significant decrease of the period – for $\lambda = 10^{-7}$ a reduction of 25% is predicted whereas the change in the volume of the drop is only 0.2% of the initial volume. As expected, the increase of the evaporation rate to $\beta = 10^{-3}$ results in a larger reduction of the period of oscillation. For this rate of evaporation approximately 2% reduction in the period is observed for $\lambda = 10^{-4}$.

Next, we consider variations of the period of oscillations with the evaporation rate β, for a fixed value of the density ratio $\lambda = 10^{-7}$ – similar results can be expected for smaller λ but larger β (see Section 2.2.1). The largest value used for evaporation rate is $\beta = 10^{-3}$ which corresponds to $\Delta T \simeq 500$°C for heptane drops in air. It is noted from Table 2 that the volume change for this value of β is somewhat significant and may have some effects on the period. This issue will be investigated later in Section 2.2.2 via comparison of the numerical results with predictions of the theory. The period values shown in Fig. 4 belong to the primary mode and are the average of the first three periods of oscillations for $Re_l = 100$ and 30. For $Re_l = 5$, the amplitude of oscillations becomes very small for these small-amplitude simulations, therefore, the first oscillation is used for period calculation.

Fig. 4(a) shows the variations of the period of oscillations for a drop released from an initial second spherical harmonic shape with an amplitude of $\epsilon_{20} = 0.05$. A significant reduction in the period is observed with the increase of the evaporation rate; up to ~80% for $\beta = 10^{-3}$. It appears from Fig. 4(a) that the rate of change of the period with the evaporation rate decreases for large values of β. For all values of β, the decrease of Re_l increases the period, however, the results suggest that the effect of the Reynolds number on the period diminishes with the increase of the evaporation rate. With the increase of β the period of oscillation decreases and less time is available for viscous dissipation.

In Figs. 4(b)–(d) variation of the period is portrayed for higher spherical modes $n = 3$, 4, and 5 with an initial disturbance amplitude of 0.05. It is observed that, similarly to non-evaporating drops, the oscillations of evaporating drops take place with smaller period for higher modes. The effect of the Reynolds number on the period is enhanced with the increase of n. In Section 2.2.1, it is shown that the kinetic energy of an oscillating drop is proportional to $(n-1)(n+2)/4(2n+1)$ which increases with the increase of n. The increase of the kinetic energy enhances the viscous effects. It is, however, observed that the effect of the Reynolds number

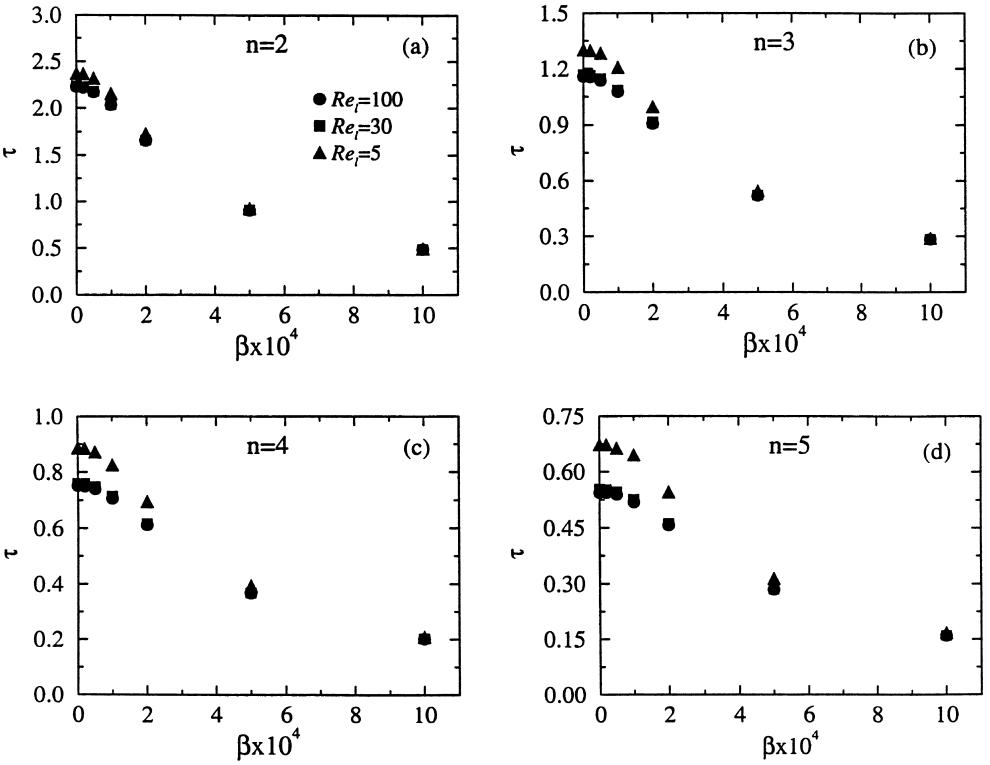

Fig. 4. Variations of the period of oscillation with evaporation rate for $\lambda = 10^{-7}$: (a) $n = 2$; (b) $n = 3$; (c) $n = 4$; (d) $n = 5$.

tends to diminish at high evaporation rates for all the modes. The general observation from Fig. 4 is the existence of a similarity in the variations of the period with β for the low evaporation rate cases considered in this subsection. This observation is verified by theory in Section 2.2.1 where we show that the period of oscillations of a slowly evaporating drop, when normalized with the period of the corresponding non-evaporating drop, is only a function of the non-dimensional parameter α and the coefficient F_n.

Previous studies (e.g., [6,16]) show that with the decrease of the Reynolds number the nature of oscillations of a non-evaporating drop changes from underdamped to overdamped. These studies also show that this transition occurs for Reynolds numbers of about unity. Fig. 5 indicates a similar behavior for an evaporating drop with $\beta = 2 \times 10^{-4}$, $\lambda = 10^{-7}$, $\epsilon_{20} = 0.05$, and $Re_l = 1$. However, analogous to the increase of the frequency of oscillations at higher Reynolds numbers, the rate of damping increases when the drop is evaporating. This could again be attributed to the increase of the kinetic energy by evaporation which enhances the viscous effects for the evaporating drop.

2.1.2. High evaporation rate

In this subsection, we briefly study the effects of high evaporation rates on the oscillation of drops to complete our investigation. This study has also the extra advantage of unmasking some of the physical phenomena which are not clearly observed at low evaporation rates.

To investigate the effects of high evaporation rate, second-mode oscillations of a drop with $\epsilon_{20} = 0.05$ are considered. The drop is allowed to evaporate with a variety of β values while the magnitude of the density ratio, λ, is chosen such that $\alpha = 0.1$ for all of the cases. In this manner, changes in the magnitude of the recoil force are due to variations of the surface curvature only. This allows us to study the modifications of the period of oscillations due mainly to changes in the drop size. Fig. 6 shows the temporal variations of the amplitude of the primary input P_2 for low and high evaporation rates. At low evaporation rate the amplitude of P_2 decreases in time due mainly to viscous effects. For the case with high evaporation rate the decay of the amplitude is much faster, in part, because the drop radius for this case decreases to ~45% of its initial value at the end of the simulation. An analysis of the plots (not shown) of the temporal variation of the amplitude normalized with instantaneous radius of the equivalent spherical drop indicated that the decay rate of the amplitude is faster than the rate of decrease of the radius.

To further investigate the period of oscillations, in Fig. 7(a) we show the variation of the period with the number of periods for a variety of β values. It is observed that, starting from an initial amplitude of 0.05, the period of oscillations of the non-evaporating drop remains the same in time. For $\beta = 10^{-4}$, the period of oscillations decreases but is again nearly constant as the number of periods increases. Further increase of β results in a pronounced variation of the period with time. For $\beta = 10^{-2}$, the highest evaporation rate considered, a significant decrease is observed in the period of oscillation as the number of periods increases. A physical explanation for changes in the period may be provided by considering a quasi-steady state oscillation for the drop, i.e., assuming that the oscillations of the drop at time t can be characterized by its instantaneous radius ϱ. Since the characteristic time for the non-evaporating drop is proportional to $(r_0)^{3/2}$, we can postulate that the period of oscillation is decreased proportional to the decrease of $\varrho^{3/2}$. In Section 2.2.1 an expression is obtained for the period of oscillations that can accurately describe the variations of the period as observed here.

It was pointed out in Section 2.1.1 that evaporation affects the oscillations by either changing the size of the drop or modifying the normal stress through the recoil force. Numerical simulation allows the investigation of

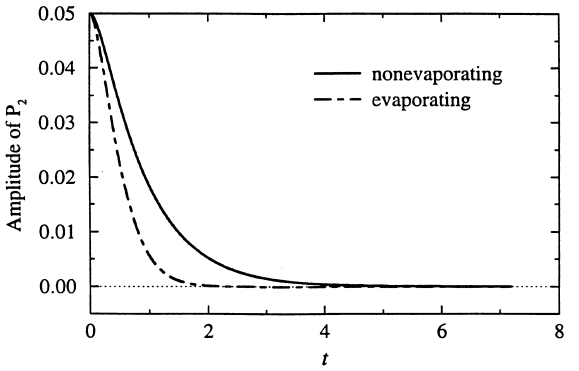

Fig. 5. Temporal variations of the amplitude of the primary input P_2 for $\epsilon_{20} = 0.05$ and $Re_l = 1$. For the evaporating case $\beta = 2 \times 10^{-4}$ and $\lambda = 10^{-7}$.

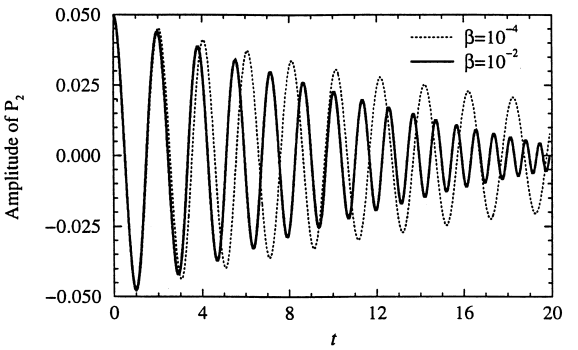

Fig. 6. Temporal variations of the amplitude of the primary input P_2 for $\epsilon_{20} = 0.05$, $Re_l = 100$, and $\alpha = 0.1$.

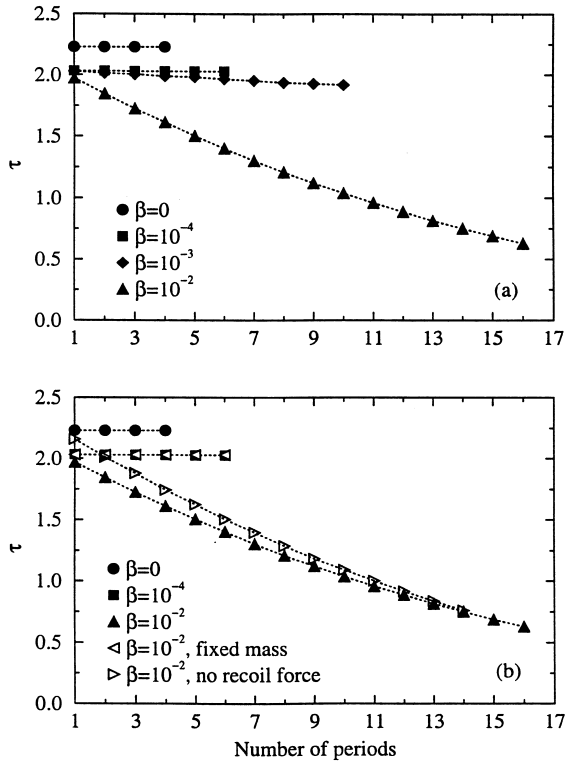

Fig. 7. Variations of the period with the number of periods for a drop with $\epsilon_{20} = 0.05$, $Re_l = 100$, and $\alpha = 0.1$.

either of the above mechanisms by setting the other one equal to zero. For drops evaporating at low rates, this decomposition revealed that the change in the drop size does not significantly affect the period of oscillations and the recoil force is responsible for the observed modifications. In Fig. 7(b), the results from a similar analysis are shown for a drop evaporating with high rate. It is observed that when the mass of the drop is fixed, the recoil force changes the period of oscillations in a manner similar to what was observed for low evaporation rate – the modification in the period is the same for all number of periods. When the recoil force is set equal to zero, however, a variation for the period with the number of periods is clearly observed. This suggests that changes in the drop size at large evaporation rate significantly affect the period of oscillations. An analysis of the data for the first few oscillations indicated that the ratio of the period for the case with high evaporation rate ($\beta = 10^{-2}$) to the period for the similar case without recoil force is close to 0.912. This is the same value obtained for the ratio of the period of a slowly evaporating drop to the period of its respective non-evaporating drop when the same value is used for α.

The results from additional simulations (not shown) indicated that the change of the period with the number of periods is smaller for higher modes of oscillations. This is due to the fact that the period of oscillation is shorter for drops oscillating at higher modes. As a result, for the same rate of evaporation, the change in the drop size during each period of oscillation becomes smaller as the mode of oscillation increases. This diminishes the effects of evaporation on the period of oscillations at higher modes.

2.2. Theory

Oscillations of an evaporating drop, in general, is a complex, nonlinear problem that demands a sophisticated analytical solution. However, the results of our numerical simulations suggest that, under the conditions considered here, the problem can be simplified. In this section, we present a theoretical analysis for infinitesimal-amplitude oscillations of an inviscid drop. The predictions of the theory are compared to the results of the numerical simulations in Section 2.2.2.

2.2.1. Period of oscillations and kinetic energy

First, we consider a solution for the period of oscillations of an inviscid, evaporating drop surrounded by an inviscid, incompressible gas. Since the radius of the drop is changing, as a result of evaporation, the basic state is time-dependent and a normal-mode analysis is not valid in an exact sense. However, as it has been the case in many other studies (see e.g., [17] and references therein), we can assume that the time scale for the evolution of the interface is much shorter than that for the basic state. In this manner, the basic state may be considered quasi-steady and a normal-mode analysis can be implemented with approximation. The validity of this assumption is later verified through the agreement observed between the theory and simulations in Section 2.2.2. The solution procedure here, is similar to that adopted by Lamb [3, pp. 474–475], for oscillations of a (non-evaporating) inviscid drop whose surface is described as

$$h = a + \epsilon_n P_n \cos(\omega t + \zeta). \tag{2.12}$$

For the quasi-steady evolution of the evaporating drop, the velocity potentials for the liquid (Φ_l) and the gas (Φ_g) can be described by the same expressions as those given by [3] for a non-evaporating drop

$$\Phi_l = -\frac{\omega a}{n}\frac{r^n}{a^n}\epsilon_n P_n \sin(\omega t + \zeta),$$

$$\Phi_g = \frac{\omega a}{n+1}\frac{a^{n+1}}{r^{n+1}}\epsilon_n P_n \sin(\omega t + \zeta). \tag{2.13}$$

The liquid and gas pressures are then, respectively, expressed as

$$p_{\mathrm{l}} = p_{\mathrm{l,eq}} + \frac{\omega^2 a}{n}\epsilon_n P_n \cos(\omega t + \zeta),$$
$$p_{\mathrm{g}} = p_{\mathrm{g,eq}} - \frac{\lambda\omega^2 a}{n+1}\epsilon_n P_n \cos(\omega t + \zeta), \tag{2.14}$$

where $p_{\mathrm{l,eq}}$ and $p_{\mathrm{g,eq}}$ refer to the equilibrium pressures attained when the drop assumes a spherical shape, i.e., for $\epsilon_n = 0$. The pressures must satisfy the normal stress boundary condition (2.3) which for inviscid drop and inviscid ambient gas reads

$$p_{\mathrm{l}} - p_{\mathrm{g}} = \mathscr{K} + \alpha F_n^2 \mathscr{K}^2 + \frac{4\alpha}{a} F_n(1-F_n)\mathscr{K} + \frac{4\alpha}{a^2}(1-F_n)^2. \tag{2.15}$$

For infinitesimal-amplitude perturbations of a drop, the curvature can be described as [3]

$$\mathscr{K} = \frac{2}{a} + \frac{(n-1)(n+2)}{a^2}\epsilon_n P_n \cos(\omega t + \zeta). \tag{2.16}$$

Substituting from (2.14) and (2.16) into (2.15) with

$$p_{\mathrm{l,eq}} - p_{\mathrm{g,eq}} = \frac{4\alpha}{a^2}(1-F_n)^2 + \left[1 + \frac{4\alpha}{a}F_n(1-F_n)\right]\frac{2}{a} + \alpha F_n^2 \frac{4}{a^2}, \tag{2.17}$$

and neglecting terms $\mathrm{O}(\epsilon_n^2)$ yields:

$$\omega^2 = \frac{1}{a^3}\left(1 + \frac{4\alpha F_n}{a}\right)\frac{n(n-1)(n+1)(n+2)}{n+1+\lambda n}. \tag{2.18}$$

The derivation leading to (2.18), demonstrates that the contribution of the pressure fluctuations of the ambient gas to the frequency of oscillation is $\mathrm{O}(\lambda)$. This justifies the neglect of these fluctuations for $\lambda \ll 1$ in formulation of Part I.

Setting $\alpha = 0$, (2.18) reduces to an expression for the frequency of oscillations of a non-evaporating drop, ω_{ne}. This yields:

$$\frac{\omega^2}{\omega_{\mathrm{ne}}^2} = \frac{a_{\mathrm{ne}}^3}{a^3}\left(1 + \frac{4\alpha F_n}{a}\right), \tag{2.19}$$

where, a_{ne} is the mean radius of the non-evaporating drop. Eq. (2.19) can be expressed as

$$\frac{\tau}{\tau_{\mathrm{ne}}} = \left(\frac{a}{a_{\mathrm{ne}}}\right)^{3/2}\left(1 + \frac{4\alpha F_n}{a}\right)^{-1/2} \tag{2.20}$$

for the ratio of the period of oscillations of an evaporating drop to that of a non-evaporating drop. Our numerical results indicate that the effects of small-amplitude oscillations on the evaporated mass are small, thus the instantaneous mean radius of the oscillating drop can be closely approximated by that of a spherical drop

$$\varrho = (1 - 4\beta t)^{1/2}. \tag{2.21}$$

Further, for infinitesimal-amplitude oscillations $a_{\mathrm{ne}} \simeq 1$, therefore, (2.20) yields

$$\frac{\tau}{\tau_{\mathrm{ne}}} = \frac{(1-4\beta t)^{3/4}}{\left[1 + 4\alpha F_n(1-4\beta t)^{-(1/2)}\right]^{1/2}}. \tag{2.22}$$

It is noted that (2.22) depends on the mode of oscillation through F_n and for low evaporation rates ($\beta \to 0$) reduces to

$$\frac{\tau}{\tau_{\mathrm{ne}}} = (1 + 4\alpha F_n)^{-1/2}, \tag{2.23}$$

which is a function of α and F_n only.

Eq. (2.22) can be used to investigate the effects of the evaporation rate and the density ratio on the period of oscillations of an evaporating drop. Fig. 8(a) shows the temporal variations of the periods ratio for $\lambda = 10^{-6}$ at different values of β for two modes of oscillation. It is observed that for $\beta \leqslant 10^{-4}$ the effect of the drop size change is small and the period of oscillations does not significantly vary in time. Oscillations of a drop with $\beta = 10^{-3}$ may still be described by neglecting the changes in the drop size. However, as the numerical results also suggest, for $\beta = 10^{-2}$ temporal variation of

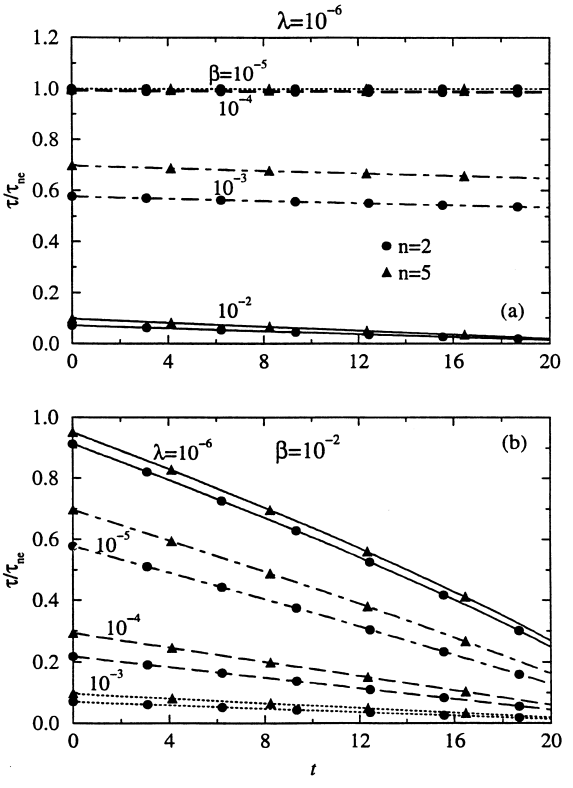

Fig. 8. Temporal variations of the period of oscillations of an evaporating drop from Eq. (2.22): (a) $\lambda = 10^{-6}$; (b) $\beta = 10^{-2}$.

the period is large as a result of the significant changes in the drop size. To investigate the effects of the density ratio at this large evaporation rate ($\beta = 10^{-2}$), in Fig. 8(b) a variety of λ values are considered. This figure shows that the temporal variations of the period is large for all the values of the density ratio. As expected, this indicates that the temporal variations of the period is dependent more on the evaporation rate than on the density ratio. A comparison of the results for $n = 5$ with those for $n = 2$ indicates that τ/τ_{ne} always increases with the increase of the mode of oscillation. All of these observations are in qualitative agreement with the numerical results and indicate that (2.22) can be used for the prediction of the period of infinitesimal-amplitude oscillations of an evaporating drop at high Reynolds numbers.

The numerical results of Section 2.1.1 and Eq. (2.23) indicate that, for low evaporation rate, the oscillations of the drop may be approximately represented by a single time-independent frequency, i.e.,

$$a_n = \epsilon_n \cos(\omega t + \zeta). \tag{2.24}$$

For quasi-steady evaporation, we can derive an expression for the kinetic energy of the drop starting from the following relation provided by Rayleigh [2]:

$$E_k = \frac{1}{2n(2n+1)}\left(\frac{da_n}{dt}\right)^2, \tag{2.25}$$

where we are only considering mode n, and E_k is normalized by the surface energy of the spherical drop $4\pi\sigma a^2$. For inviscid drop and small evaporation rates the amplitude of oscillations ϵ_n can also be assumed independent of time. With this assumption, substituting from (2.24) into (2.25) yields

$$E_k = \frac{\omega^2}{2n(2n+1)}\epsilon_n^2[\sin(\omega t + \zeta)]^2, \tag{2.26}$$

which may also be expressed as

$$E_k = \frac{\omega^2}{4n(2n+1)}\epsilon_n^2\{1 - \cos[2(\omega t + \zeta)]\}, \tag{2.27}$$

indicating that the frequency of oscillations of the kinetic energy is twice as large as that of the surface of the drop. This is in agreement with physical intuition as the kinetic energy assumes minimum values when the drop surface reaches its maximum deformation, occurring twice within each period of surface oscillation. Previous studies of non-evaporating drops as well as our numerical results show that viscous effects in the oscillations may be well represented by implementing a "decay factor" Γ, such that $\epsilon_n = \epsilon_{n0}\exp(-\Gamma t)$. Therefore, for low evaporation rates, we may extend (2.26) to an expression for the kinetic energy of a viscous drop by including a decay factor

$$E_k = \frac{1}{2n(2n+1)}\epsilon_{n0}^2[\omega \sin(\omega t + \zeta) + \Gamma \cos(\omega t + \zeta)]^2 \exp(-2\Gamma t). \tag{2.28}$$

For small viscosity, Γ is small in comparison to ω and (2.28) is simplified to

$$E_k = \frac{\omega^2}{4n(2n+1)}\epsilon_{n0}^2\{1 - \cos[2(\omega t + \zeta)]\}\exp(-2\Gamma t). \tag{2.29}$$

The numerical results of Section 2.1.1 show that for moderate and high Reynolds numbers Γ does not significantly change with evaporation rate. Therefore, substituting for ω from (2.18) with $a \simeq 1$, (2.29) indicates that the amplitude of oscillations of E_k for an evaporating drop is $(1 + 4\alpha F_n)$ times as large as that for a non-evaporating drop.

2.2.2. Comparison of theory with simulation

First, we consider cases with low evaporation rates for which the oscillations do not vary significantly in time and may be represented by a single value for the period. In Fig. 9, the predictions of the theory (lines) for the period ratio (2.23) are compared to the results of numerical simulations (symbols) from Section 2.1.1. Various oscillation modes are considered with an initial amplitude of 0.05. At high and moderate Reynolds numbers ($Re_l = 100$ and 30) the agreement between the theory and simulation is excellent. This is encouraging as the theory is developed for inviscid drops. Some deviations are observed for $Re_l = 5$ for which the theory overpredicts the numerical results. The deviation is larger for higher spherical modes for which the drop oscillates faster and experiences a larger viscous dissipation. The agreement observed in Fig. 9 shows that the neglect of the drop size variation has very little impact on the prediction of the period ratio. The numerical results are also in agreement with theory in that the increase of the mode of oscillation results in the increase of the period ratio. It must be added that when the inviscid theory is used for oscillations of a low Reynolds number drop the predicted period is in somewhat significant error (about 10% for $Re_l = 5$ in non-evaporating case with $n = 2$). However, Fig. 9 shows that the ratio of the period is reasonably well predicted by the theory even for low Reynolds numbers.

In Fig. 10 the prediction of the theory (2.29) is compared to the kinetic energy calculated from numerical simulations for a case with $\epsilon_{20} = 0.01$ and $Re_l = 100$. Both non-evaporating ($\beta = 0$) and evaporating ($\beta = 10^{-4}$, $\lambda = 10^{-7}$) are considered. For this low evaporation rate case, a value for Γ is calculated from numerical results using

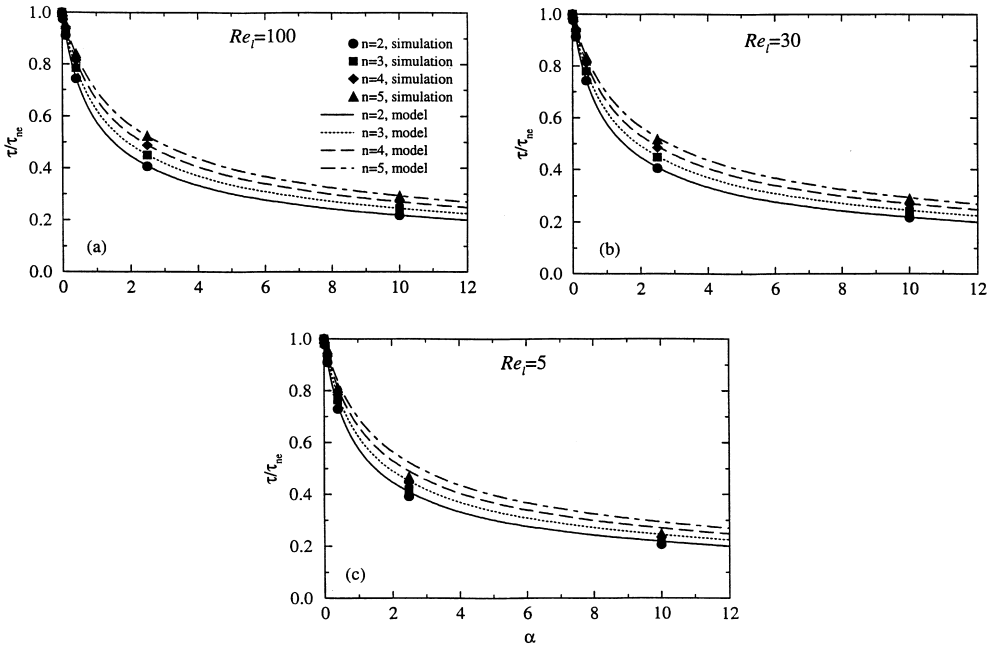

Fig. 9. Comparison between the prediction of theory (lines) and the results of numerical simulations (symbols) for the period of oscillation of a drop released with an initial amplitude of 0.05 and $\lambda = 10^{-7}$. (a) $Re_l = 100$, (b) $Re_l = 30$, and (c) $Re_l = 5$.

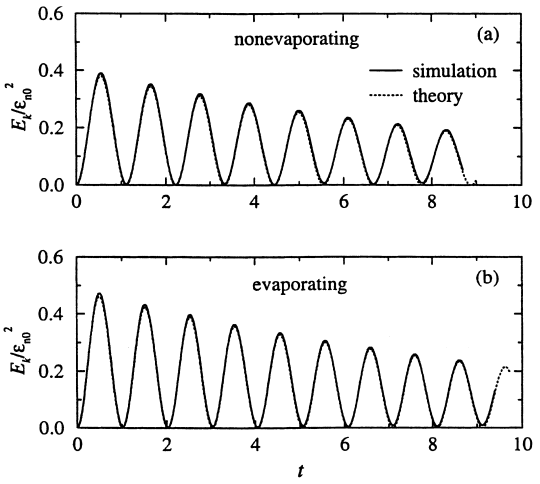

Fig. 10. Comparison between the prediction of theory and the results of numerical simulations for the kinetic energy of a drop released with $\epsilon_{20} = 0.01$ and $Re_l = 100$: (a) non-evaporating; (b) evaporating with $\beta = 10^{-4}$ and $\lambda = 10^{-7}$.

$$\Gamma_j = \frac{1}{t_j - t_{j-1}} \ln \frac{A_{j-1}}{A_j}, \quad j = 1, 2, \ldots, \tag{2.30}$$

where A represents the amplitude of the primary input and j refers to the oscillation number. The value used for Γ is the average over the first three oscillations in order to diminish the effects of the initial conditions. The kinetic energy is calculated relative to the surface energy of the equivalent spherical drop, $4\pi\sigma r_0^2$, using

$$E_k = \frac{1}{4} \int_0^{\pi} \int_0^{h} (u_l^2 + v_l^2) r^2 \sin\phi \, dr \, d\phi. \tag{2.31}$$

It is clearly observed from Fig. 10 that the theory is in good agreement with numerical results. The increase of both the amplitude and the frequency of oscillations of E_k due to evaporation is accurately predicted by the theory.

Finally, we consider the cases with high evaporation rate discussed in Section 2.1.2. In Fig. 11 the prediction of (2.22) is compared to the results of numerical simulations for $n = 2$ and 4 with the initial amplitude of 0.05, $Re_l = 100$, $\beta = 10^{-2}$, and $\alpha = 0.1$. To make the comparison, a time must be assigned to each period calculated from numerical simulations. As the best approximation the average time is used, i.e., if a period extends from t_1 to t_2, $(t_1 + t_2)/2$ is assigned to that period. In Fig. 11, the time axis is normalized by τ_{ne} for each respective mode of oscillation. Although (2.22) is obtained based on several assumptions, an excellent agreement with the numerical results is observed in Fig. 11.

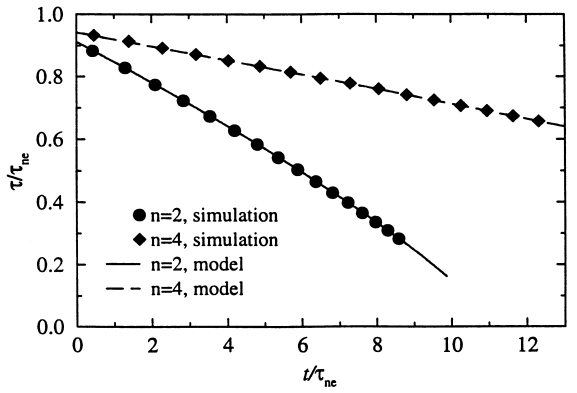

Fig. 11. Comparison between the prediction of theory (lines) and the results of numerical simulations (symbols) for the period of oscillation of a drop evaporating at high rates and released with an initial amplitude of 0.05, $Re_l = 100$, $\beta = 10^{-2}$, and $\alpha = 0.1$. The time axis for each case is normalized with the period of oscillations for the respective non-evaporating drop.

3. Effects of oscillations on evaporation

To assess the effects of oscillations on evaporation, an expression is derived for the temporal variations of the volume $V(t)$ of an evaporating, inviscid drop oscillating with infinitesimal-amplitude. With the evaporation model of Part I, the rate of change of the drop volume is described as

$$\frac{\mathrm{d}V}{\mathrm{d}t} = -\beta \int_{\Omega} \left[F_n \mathscr{K} + \frac{2}{R_n}(1 - F_n) \right] \mathrm{d}\Omega, \tag{3.1}$$

where Ω is the surface area of the drop. In accordance with numerical simulations, we represent the surface of the drop by

$$h = R_n(1 + a_n P_n), \tag{3.2}$$

where a_n, the amplitude of oscillation, is a function of time only. For a surface defined by (3.2), the curvature is given by [5]

$$\mathscr{K} = \frac{2}{R_n} + \frac{(n-1)(n+2)}{R_n} a_n P_n. \tag{3.3}$$

Substituting (3.3) into (3.1) and describing $\mathrm{d}\Omega$ in terms of h and ϕ yields

$$-\frac{1}{\beta}\frac{\mathrm{d}V}{\mathrm{d}t} = \frac{2}{R_n}\mathscr{I}_1 + \frac{(n-1)(n+2)}{R_n} F_n a_n \mathscr{I}_2, \tag{3.4}$$

where

$$\mathscr{I}_1 = 2\pi \int_0^{\pi} \left(h^2 + \frac{1}{2}h_{\phi}^2 \right) \sin\phi \, \mathrm{d}\phi,$$

$$\mathscr{I}_2 = 2\pi \int_0^{\pi} P_n \left(h^2 + \frac{1}{2}h_{\phi}^2 \right) \sin\phi \, \mathrm{d}\phi. \tag{3.5}$$

After some algebraic manipulations, detailed in the Appendix A, we arrive at

$$-\frac{1}{\beta}\frac{\mathrm{d}V}{\mathrm{d}t} = 8\pi R_n + \frac{(n^2+n+2) + 2(n-1)(n+2)F_n}{(2n+1)} \times 4\pi R_n a_n^2 + \mathrm{O}(a_n^3). \tag{3.6}$$

Describing a_n by (2.24), yields

$$-\frac{1}{\beta}[V(t) - V_0] = 8\pi R_n t + \frac{(n^2+n+2) + 2(n-1)(n+2)F_n}{(2n+1)} \times 4\pi R_n \epsilon_n^2 \int_0^t [\cos(\omega t')]^2 \, \mathrm{d}t', \tag{3.7}$$

where $V_0 = 4\pi/3$ is the initial volume of the drop. For low evaporation rates ($a \simeq 1$), we approximate the frequency of oscillation ω from (2.18), therefore

$$\frac{V_0 - V(t)}{V_0} = 6R_n\beta t + \frac{3[(n^2+n+2) + 2(n-1)(n+2)F_n]}{2(2n+1)} R_n \epsilon_n^2 \beta t + \frac{3[(n^2+n+2) + 2(n-1)(n+2)F_n]}{4(2n+1)\omega} R_n \epsilon_n^2 \beta \sin(2\omega t) + \mathrm{O}(\epsilon_n^3) + \mathrm{O}(\beta t)^2. \tag{3.8}$$

The first term on the right-hand side of (3.8) is an approximation $[\mathrm{O}(\beta t)^2]$ of the relative change in the volume of a spherical ($\epsilon_n = 0$) drop. The second and third terms on the right-hand side represent the modification in evaporation due to the surface deformation. These terms are quadratic in ϵ_n and increase with the increase of n, in agreement to the results presented in Part I. The third term on the right-hand side shows that the volume of the drop oscillates in time with a frequency twice as large as the frequency of the surface oscillation.

Further insight into the effects of oscillations on the rate of change of the mass of the drop, $\dot{M} = -\rho_l \, \mathrm{d}V/\mathrm{d}t$, is provided by rewriting (3.6) as

$$\delta\dot{M} = \frac{\dot{M} - \dot{M}_{\mathrm{sp}}}{\dot{M}_{\mathrm{sp}}} = G_n \epsilon_n^2 [1 + \cos(2\omega t)] + \mathrm{O}(\epsilon_n^3), \tag{3.9}$$

where

$$G_n = \frac{(n^2+n+2) + 2(n-1)(n+2)F_n}{4(2n+1)}. \tag{3.10}$$

According to (3.9), the evaporation rate of the oscillating drop exhibits an oscillatory behavior, however, it is always greater than or equal to the evaporation rate of a spherical drop. It is also noted that $\delta\dot{M}$ varies quadratically with the amplitude of oscillations. When integrated and averaged over one period of oscillations, $\delta\dot{M} = G_n\epsilon_n^2$ which is half of that for a non-oscillating drop deformed with the same amplitude. Therefore, it

Table 3
Variations of G_n, H_n, and their ratio with the mode of oscillations

n	G_n	H_n	G_n/H_n
2	0.600	0.400	1.500
3	0.781	0.500	1.561
4	0.929	0.611	1.521
5	1.065	0.727	1.465
6	1.196	0.846	1.413
7	1.324	0.967	1.369
8	1.450	1.088	1.332

may be concluded that oscillations of the drop tend to diminish the increase in the evaporation rate (caused by surface deformation) by 50%. This is due mainly to the change in the amplitude of the surface deformation during oscillations. For a viscous drop, the decrease is expected to be larger than 50% due to the decay of amplitude in time. The effect of the mode of oscillations, is realized by examining G_n values in Table 3 which indicate a nearly linear increase with n. It is emphasized that, (3.9) does not include the effect of change in the radius of the drop on the evaporation rate. However, this should not significantly affect this analysis as we are considering the deviation from the equivalent spherical drop.

At this point, it is instructive to consider the change in the surface area of the drop during oscillations. The surface area, A, is given by the integral $\mathscr{I}_1$ in (3.5), and its deviation from the surface of a spherical drop can be expressed as:

$$\delta A = \frac{A - A_{\mathrm{sp}}}{A_{\mathrm{sp}}} = H_n \epsilon_n^2 [1 + \cos(2\omega t)] + \mathrm{O}(\epsilon_n^3), \tag{3.11}$$

where

$$H_n = \frac{(n^2 + n + 2)}{4(2n + 1)}. \tag{3.12}$$

The change in the surface area is similar to the change in the evaporated mass. The H_n values listed in Table 3 show that the surface area also increases with the increase of the mode of oscillation. However, the ratio G_n/H_n is larger than unity for all modes, which indicates that the increase in the evaporated mass is not due to the increase in the surface area only. It is interesting that this ratio has a peak value of 1.561 for $n = 3$ and then decreases with the increase of n.

4. Conclusion

Numerical simulation and theoretical analysis are used to investigate free oscillations of evaporating drops. The preheat period is not considered and the drop is assumed to be at the liquid boiling temperature. The surrounding gas, except for the region close to the drop, is also at a uniform temperature and its density is much smaller than the liquid density. Under these assumptions, it is shown that the gas and the liquid phase can be studied separately. The coupling between the two phases is through an evaporation model which is derived from the study of the gas phase in Part I and is then implemented to analyze the oscillations in the liquid phase.

The use of the model has limited the analysis to small disturbance amplitudes. The effects of the mode of the initial surface disturbance, the Reynolds number, the transfer number, and the density ratio are studied. Evaporation affects oscillations by decreasing the size of the drop and/or through the recoil force appearing in the normal stress boundary condition on the interface. The results of the numerical simulations are discussed for low and high evaporation rates, where low evaporation rates are characterized by somewhat insignificant changes in the drop size. The period of oscillations of a drop evaporating with low rates may significantly change as a result of the recoil force. In general, the period of oscillations is decreased with the increase of the evaporation rate. For high evaporation rates, the period of oscillations also varies in time due to significant reduction in the drop size. Similar trends for the variations of the period with the evaporation rate are observed for the second-, third-, fourth-, and fifth-mode surface disturbances at high and moderate Reynolds numbers. At very low Reynolds numbers the nature of oscillations is changed to underdamped, similar to oscillations of non-evaporating drops.

The theoretical analysis is based on infinitesimal-amplitude oscillations. For the period of oscillations of the evaporating drop, a normal-mode analysis is performed by assuming that the time scale for the evolution of the basic state is much larger than the time scale for the evolution of the drop surface. The theory describes the ratio of the period of oscillations of an evaporating drop to the period of oscillations of the respective non-evaporating drop as a function of the mode of oscillation, the evaporation rate, and the density ratio. A comparison of the prediction of the theory with numerical results indicates excellent agreements for both low and high evaporation rates. The variations of the kinetic energy, for low evaporation rates, is also predicted by the theory and show reasonable agreements with numerical results.

Finally, the effect of oscillations on evaporation is investigated by theory. It is shown that the rate of evaporation of an oscillating drop varies in time but it is always greater than or equal to the rate of evaporation of the equivalent spherical drop. The increase in the evaporation rate is proportional to the square of the surface disturbance amplitude and is larger for higher

modes. When compared to a non-oscillating deformed drop at the same surface disturbance amplitude, oscillations decrease the rate of evaporation. It is also shown that the change in the evaporation rate is larger than the change of the surface area resulted from surface deformation.

While the present study provides new insights into evaporation of deformed drops and oscillations of evaporating drops, due to the limitations of the evaporation model, the final analysis on the modification of the evaporation rate is restricted to small disturbance amplitudes. Nevertheless, the analysis indicates that the modification in the evaporation rate is enhanced quadratically with the increase of the amplitude of oscillations, and warrants a future study that allows consideration of large amplitudes. It should be added that the main assumptions invoked for this study, are similar to those adopted in the classical derivation of the d^2-law. Given the success of this law in prediction of evaporation rate for spherical drops in many cases of practical interest, we can expect that the results of the current study can also be used, with reasonable approximations, in practice. A main issue in the practical application, however, is a judicious choice of mean property values based on the temperature range of concern.

Acknowledgements

The support for this work was provided by the National Science Foundation under Grant CTS-9874655 with Dr. M.C. Roco as Program Director and by the US Office of Naval Research under Grant N00014-99-1-0808 with Dr. G.D. Roy as Technical Monitor.

Appendix A

In this appendix, evaluation of integrals $\mathscr{I}_1$ and $\mathscr{I}_2$ of Section 3, is described

$$\mathscr{I}_1 = 2\pi\mathscr{I}_{11} + \pi\mathscr{I}_{12},$$
$$\mathscr{I}_{11} = \int_0^\pi h^2 \sin\phi \, \mathrm{d}\phi, \quad \mathscr{I}_{12} = \int_0^\pi h_\phi^2 \sin\phi \, \mathrm{d}\phi. \tag{A.1}$$

Substituting $\mu = \cos\phi$ in (A.1) yields

$$\mathscr{I}_{11} = R_n^2 \int_{-1}^{1} (1 + a_n P_n)^2 \, \mathrm{d}\mu = 2R_n^2 + 2(2n+1)^{-1} R_n^2 a_n^2, \tag{A.2}$$

$$\mathscr{I}_{12} = R_n^2 a_n^2 \int_{-1}^{1} (1-\mu^2) \left(\frac{\mathrm{d}P_n}{\mathrm{d}\mu}\right)^2 \mathrm{d}\mu = 2n(n+1)(2n+1)^{-1} R_n^2 a_n^2, \tag{A.3}$$

$$\mathscr{I}_1 = 4\pi R_n^2 + 2\pi(2n+1)^{-1}(n^2+n+2) R_n^2 a_n^2. \tag{A.4}$$

Similarly

$$\mathscr{I}_2 = 2\pi\mathscr{I}_{21} + \pi\mathscr{I}_{22},$$
$$\mathscr{I}_{21} = \int_0^\pi P_n h^2 \sin\phi \, \mathrm{d}\phi,$$
$$\mathscr{I}_{22} = \int_0^\pi P_n h_\phi^2 \sin\phi \, \mathrm{d}\phi, \tag{A.5}$$

$$\mathscr{I}_{21} = R_n^2 \int_{-1}^{1} P_n (1 + a_n P_n)^2 \, \mathrm{d}\mu = 4(2n+1)^{-1} R_n^2 a_n + R_n^2 a_n^2 \int_{-1}^{1} P_n^3 \, \mathrm{d}\mu, \tag{A.6}$$

$$\mathscr{I}_{22} = R_n^2 a_n^2 \int_{-1}^{1} P_n (1-\mu^2) \left(\frac{\mathrm{d}P_n}{\mathrm{d}\mu}\right)^2 \mathrm{d}\mu = n(n+1) R_n^2 a_n^2 \int_{-1}^{1} P_n^3 \, \mathrm{d}\mu, \tag{A.7}$$

$$\mathscr{I}_2 = 8\pi(2n+1)^{-1} R_n^2 a_n + \pi(n^2+n+2) R_n^2 a_n^2 \int_{-1}^{1} P_n^3 \, \mathrm{d}\mu. \tag{A.8}$$

References

[1] F. Mashayek, Dynamics of evaporating drops. Part I: formulation and evaporation model, Int. J. Heat Mass Transfer 44 (2001) 1517–1526.
[2] W.S. Rayleigh, On the capillary phenomena of jets, Proc. R. Soc. Lond. 29 (1879) 71–97.
[3] H. Lamb, Hydrodynamics, sixth ed., Cambridge University, Cambridge, 1932.
[4] S. Chandrasekhar, The oscillations of a viscous liquid globe, Proc. Lond. Math. Soc. 9 (3) (1959) 141–149.
[5] W.H. Reid, The oscillations of a viscous liquid drop, Q. Appl. Math. 18 (1960) 86–89.
[6] A. Prosperetti, Free oscillations of drops and bubbles: the initial-value problem, J. Fluid Mech. 100 (1980) 333–347.
[7] J.A. Tsamopoulos, R.A. Brown, Nonlinear oscillations of inviscid drops and bubbles, J. Fluid Mech. 127 (1983) 519–537.
[8] G.B. Foote, A numerical method for studying simple drop behavior: simple oscillation, J. Comput. Phys. 11 (1973) 507.
[9] C.T. Alonso, The dynamics of colliding and oscillating drops, in: D.J. Collins, M.S. Plesset, M.M. Saffren (Eds.), Proceedings of the International Colloquium on Drops and Bubbles, Jet Propulsion Laboratory, Pasadena, CA, 1974.
[10] T.S. Lundgren, N.N. Mansour, Oscillations of drops in zero gravity with weak viscous effects, J. Fluid Mech. 194 (1991) 479–510.
[11] F. Mashayek, N. Ashgriz, Nonlinear oscillations of drops with internal circulation, Phys. Fluids 10 (5) (1998) 1071–1082.
[12] E.H. Trinh, T.G. Wang, Large-amplitude free and driven drop shape oscillations: experimental observations, J. Fluid Mech. 122 (1982) 315–338.

[13] E. Becker, W.J. Hiller, T.A. Kowalewski, Experimental and theoretical investigation of large amplitude oscillations of liquid droplets, J. Fluid Mech. 231 (1991) 180–210.
[14] T.G. Wang, A.V. Anilkumar, C.P. Lee, Oscillations of liquid drops: results from USML-1 experiments in space, J. Fluid Mech. 308 (1996) 1–14.
[15] E.H. Trinh, D.B. Thiessen, R.G. Holt, Driven and freely decaying nonlinear shape oscillations of drops and bubbles immersed in a liquid: experimental results, J. Fluid Mech. 364 (1998) 253–272.
[16] F. Mashayek, N. Ashgriz, A spine-flux method for simulating free surface flows, J. Comput. Phys. 122 (1995) 367–379.
[17] Z.W. Lian, R.D. Reitz, The effect of vaporization and gas compressibility on liquid jet atomization, Atomization and Sprays 3 (3) (1993) 249–264.